Nuclear Engineering and Technology 52 (2020) 1110–1119

Contents lists available at ScienceDirect

Nuclear Engineering and Technology

journal homepage: www.elsevier.com/locate/net

Original Article

Performance evaluation of the Floating Absorber for Safety at Transient (FAST) in the innovative Sodium-cooled Fast Reactor (iSFR) under a single control rod withdrawal accident

Seongmin Lee, Yong Hoon Jeong*

Korea Advanced Institute of Science and Technology, 291 Daehak-ro, Yuseong-gu, South Korea

ARTICLE INFO

Article history:
Received 5 June 2019
Received in revised form
17 October 2019
Accepted 9 November 2019
Available online 11 November 2019

Keywords:
FAST
FASTAC
iSFR

ABSTRACT

The Floating Absorber for Safety at Transient (FAST) is a safety device used in the innovative Sodium-cooled Fast Reactor (iSFR). The FAST insert negative reactivity under transient or accident conditions. However, behavior of the FAST is still unclear under transient conditions. Therefore, the existing Floating Absorber for Safety at Transient Analysis Code (FASTAC) is improved to analyze the FAST movement by considering the reactivity and temperature distribution within the reactor core. The current FAST system is simulated under a single control rod withdrawal accident condition. In this investigation, the reactor thermal power does not return to its initial thermal power even if the FAST inserts negative reactivity. Only a 9 K of coolant temperature margin, in the hottest fuel assembly at EOL, can lead to unnecessary insertion of the negative reactivity. On the other hand, the FASTs cannot contribute to controlling the reactivity when normalized radial power is less than 0.889 at BOL and 0.972 at EOL. These simulation results suggest that the current FAST design needs to be optimized depending on its installed location. Meanwhile, the FAST system keeps the fuel, cladding and coolant temperatures below their limit temperatures with given conditions.

1. Introduction

The Floating Absorber for Safety at Transient (FAST) is designed to be used in the Innovative Sodium-cooled Fast Reactor (iSFR) [1]. This reactor is one of the Sodium-cooled Fast Reactors (SFRs) based on the design of Prototype Generation-IV Sodium-cooled Fast Reactor (PGSFR). Given that the newly developed fuel recycling technology is not available for the PGSFR, iSFR is designed to operate with low enriched uranium (LEU) fuel that gradually turns into plutonium-dominant fuel. As inherent safety features, iSFR has negative reactivity coefficients to ensure the negative feedback effect under transient conditions. With a moderating ratio of 0.89, sodium is a non-moderating material compared to water with a ratio of 62. Generally, the coolant temperature coefficient (CTC) is negative or slightly positive depending on the fast reactor design and fuel burnup. However, even if the rise in system temperature results in a neutron hardening effect [2], the overall reactivity feedback coefficient is negative thanks to the help of other negative reactivity coefficients, including the dominant Doppler feedback effect [3]. Sodium, however, acts as a neutron absorber or reflector, thus inserting positive reactivity into the reactor when voids are generated. The value of the coolant void reactivity (CVR) is used to assess the safety of the fast reactors, assuming the voids cover the active core region. In iSFR, CVR tends to become greater as an inventory of transuranic compositions increases. The value of CVR is slightly negative at the beginning of life (BOL), but approximately 756 cents at the end of life (EOL). Therefore, it is desirable to lower the value of CVR to mitigate the risk of an accident in the nuclear power plant.

Many researchers have tried to overcome the sodium void effect, which can increase the reactor thermal power. Merk [4] reduced the sodium void effect by using moderating material, such as zirconium hydride, for the cladding layer to enhance the safety characteristics of SFR without changing the reactor core design. Kim et al. [5] attempted to maintain the sodium void worth low with a pan-shape core design that has two different heights of fueled region. Sociora et al. [6] carried out an analysis focusing on the absorption or leakage in components and were able to reduce

* Corresponding author.
E-mail addresses: seongmeen@kaist.ac.kr (S. Lee), jeongyh@kaist.ac.kr (Y.H. Jeong).

https://doi.org/10.1016/j.net.2019.11.011

the sodium void worth by placing a fertile blanket above and below the core assembly; however, they had to increase the neutron leakage which deteriorates the neutron economy.

On the other hand, Hartanto et al. [1] proposed a passive safety device called FAST to solve the problems of CVR without neutron leakage in normal operation. The FAST can be equipped with a 95% enriched B_4C neutron absorber. The FAST density can be determined by adjusting the volume portion of the void region. The absorber placed at the bottom of the FAST inserts negative reactivity into the reactor core at the moment when the buoyancy acting on its body is less than the gravity. Because the buoyancy depends on the coolant temperature, the change in its temperature enables the FAST to sink and to reduce reactor thermal power. According to their results [1], the FAST passively reduced 235 cents of CVR at BOL and 320 cents of CVR at EOL when 20% of boron-10 was depleted. The small bypass holes allow the coolant to pass through them during a loss of coolant accident (LOCA), causing the FAST to fall to the bottom by gravity. The flow rate through the holes is insensitive to the flow in subchannels because the flow direction is perpendicular to the interface between the subchannel and the bypass holes. Additionally, the FAST can be mounted in the position of the fuel rod and the number of the FASTs is determined by the reactivity worth required in the reactor system. Therefore, iSFR can easily adopt the FAST system without modifying the reactor geometry to increase neutron leakage.

Fig. 1 shows the behavior of the FAST under the steady-state as well as transient conditions. The initial density of FAST enables the FAST to float in the coolant. Therefore, it is located outside the active core region in normal operation conditions. If transient conditions increase the coolant temperature, then the FAST falls into the active core and inserts negative reactivity. In an accident such as LOCA, the FAST falls regardless of the coolant density because the coolant leaks through the bottom bypass holes.

A number of studies have sought to analyze the behavior of the falling cylinder. Khalil et al. [7] presented an analytical solution for the velocity distribution in the side region of the moving cylinder. They calculated the drag from the velocity distribution in both fully developed regions and the entrance regions. Kim et al. [8] measured disturbance region and the fully developed region when the long cylinder with hemispherical ends reached its terminal velocity. They concluded that the disturbance region is approximately 6% of the total length of the cylinder. Because of the very short disturbance region, the shear stress acting on the cylinder wall is not significantly different from the shear stress applied to the cylinder when the flow regime is fully developed along the cylinder length. Wehbeh et al. [9] focused on the influence of the radial flow at the end of the cylinder for the terminal velocity. They

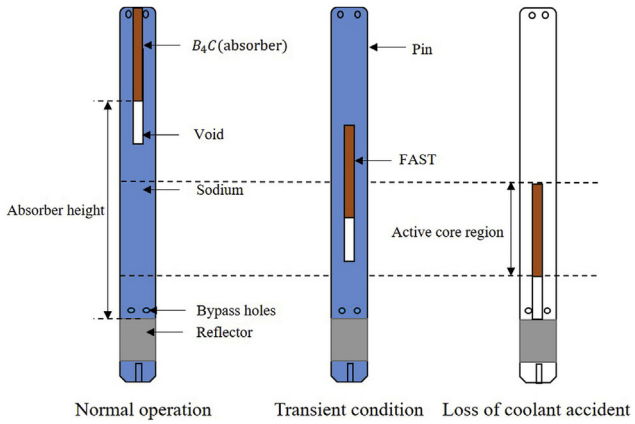

Fig. 1. Behavior of the FAST under the steady-state, transient and LOCA conditions.

estimated the fluid velocity around the cylinder when it reached the terminal velocity. In their results, the radial flow effect on the cylinder end is determined by the diameter of the outer cylinder, the diameter and length of the inner cylinder. If the FAST falls in the fluid, then it may not fall to the centerline of a pin. Chen et al. [10] studied the effect of eccentricity on the cylinder velocity, and this effect was evaluated by considering the diameter ratio of the container and the cylinder. According to their results, the terminal velocity ratio of the cylinder increased as the eccentricity ratio increased.

The movements of the FAST must be properly analyzed because the FAST increases or decreases the reactor thermal power by reactivity insertion. Hartanto et al. [1] analyzed the movements of the FAST considering only buoyancy and gravity without drag and pressure forces. As the drag and pressure forces are crucial factors interfering with the movement of the FAST, Lee and Jeong [11] have developed the Floating Absorber for Safety at Transient Analysis Code (FASTAC), considering all forces acting on the FAST. The FASTAC was verified with commercial computational fluid dynamics code by comparing resistance acting on the body. Additionally, the code was successfully validated by simplified experiments where the terminal velocity was measured with various density difference conditions between the coolant and the FAST. In their experiments, they attached small guide wings to the end surface of the FAST in order to guide it to fall in the centerline of a pin because the unstable flow in the top region of the FAST can cause eccentricity. They found that approximately 1% of manufacturing tolerance of the diameter affects approximately 7% of terminal velocity. Comparatively, the guide wings, which occupy approximately 1% of the total volume, had a negligible impact on the FAST movement.

The main purpose of this study is to investigate the feasibility of the FAST system before applying the FAST system to iSFR in transient conditions. In this work, the previously mentioned FASTAC was improved by considering the transient momentum equation, temperature distribution and reactivity analysis models. In particular, the current FASTs have been simulated under a single control rod withdrawal accident, which is one of the design basis accidents (DBAs) that increase the reactor thermal power.

2. Movement analysis of the FAST

2.1. Fluid velocity model

The FAST is a passive safety device that operates depending on the coolant temperature. When the coolant temperature rises, the FAST begins to move and pushes the surrounding fluid. When the reactor is in steady-state conditions, only buoyancy and gravity act on the FAST. As the FAST begins to move, the surrounding fluid applies the drag and pressure force to the FAST. The fluid mainly flows to the side area in proportion to the FAST speed, thereby interfering with the FAST movement and delaying its speed. In this section, the fluid velocity field around the FAST is described to estimate the forces acting on its body, and models are introduced to describe each force in detail.

Fig. 2 shows the whole domain including the FAST, pin, and coolant region. The length of FAST is L, and the radius of FAST is r_F. The radius of the pin containing the coolant is r_p. When the FAST falls with velocity V_F, it pushes stationary coolant to have a velocity distribution $V_z(r)$ in the side area.

The forces acting on the FAST determine the movement of the fluid. To evaluate the fluid velocity distribution, the fluid is assumed to be incompressible, irrotational, and the flow regime is fully developed. According to Kim et al. [8], the fully developed region of the coolant along the cylinder length accounts for approximately 94% of the total length of the cylinder. They found that 6% of the

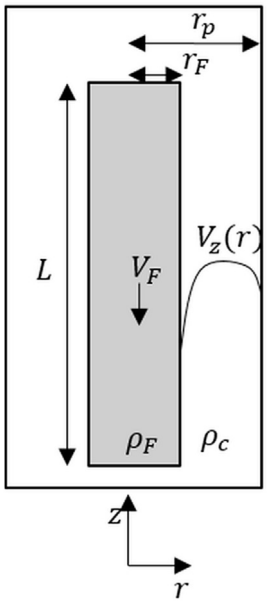

Fig. 2. Schematics of the simplified FAST, pin and coolant.

disturbance zone is sufficiently small enough to be considered as a fully developed condition for calculating wall shear stress on the cylinder body surface. The current design length of the FAST is approximately 350 times longer than the pin radius. Thus, the effect of the radial flow was neglected at both ends of the FAST [9]. Besides, the FAST was assumed to sink in the middle of the pin without the help of any device. Based on these assumptions, the axial velocity distribution was obtained with the momentum equation in cylindrical coordinates.

$$\rho_c \frac{\partial V_z}{\partial t} = -\frac{\partial P}{\partial z} + \mu\left[\frac{1}{r}\frac{\partial}{\partial r} r \frac{\partial V_z}{\partial r}\right] \tag{1}$$

where μ is the coolant viscosity, and V_z is an axial velocity function. Referring to Khalil et al. [7], the implicit forward differencing in time and central differencing in the radial direction are applied to Eq. (1) to numerically calculate the axial velocity distribution.

$$V_z(r_F) = V_F$$

$$V_z(r_p) = 0 \tag{2}$$

Eq. (2) presents boundary conditions that the fluid velocity is zero at the cylinder wall due to the no-slip condition during the FAST falls with velocity V_F. The FAST velocity V_F is defined by the resultant force including buoyancy, gravity, drag and pressure force. A detailed description of these forces is given in subsection 2.2.

$$Q = \pi r_F^2 V_F \tag{3}$$

$$Q_e = \int_{r_F}^{r_p} 2\pi r V_z(r) dr \tag{4}$$

When the FAST moves with the velocity V_F, it generates volumetric flow rate Q pushed by the FAST (Eq. 3. The volumetric flow rate Q_e numerically obtained by Eq. (4) should be equal to Q because the coolant pushed by the FAST flows into the side area of FAST. When the transient momentum equation is solved numerically, the volumetric flow can be calculated with a pressure gradient correction technique [12]. This technique adjusts the value of the pressure gradient until the difference between Q_e and Q is less than the tolerance of 10^{-6}. Following the pressure gradient correction technique, the axial velocity distribution V_z for the next time step is obtained by solving the momentum equation numerically for the whole simulation time.

2.2. Four-force model: buoyancy, gravity, drag and pressure force

There are four forces acting on the FAST. Among them, buoyancy and gravity always act regardless of the FAST movement, while the drag and pressure force are valid only when the FAST moves. Because the coolant density depends on the core height, the buoyancy acting on the FAST depends on the FAST location.

$$F_B = \int \rho_c(z) g dV \tag{5}$$

As described by Eq. (5), the buoyancy F_B acting on the FAST depends on the coolant density ρ_c and the FAST volume V. If the buoyancy acting on FAST is less than the gravity, the FAST starts to fall. Therefore, the buoyancy determines the time that the FAST begins to move.

$$F_G = \rho_F g V \tag{6}$$

where the FAST density ρ_F and fluid density ρ_c denote the FAST density and coolant density, respectively. Unlike buoyancy, gravity F_G is always constant unless the FAST density and volume change (Eq. (6)). In this investigation, the thermal expansion effect of FAST is not considered so that gravity is completely dependent on the initial mass of FAST.

$$F_D = \mu \frac{dV_z(r)}{dr} A_s \Big|_{r=r_F} \tag{7}$$

Drag F_D is represented by Eq. (7) assuming that the flow is fully developed along the FAST length. The fluid has different velocities along the radial direction because of the boundary conditions. The drag is proportional to the viscosity and velocity gradient of the

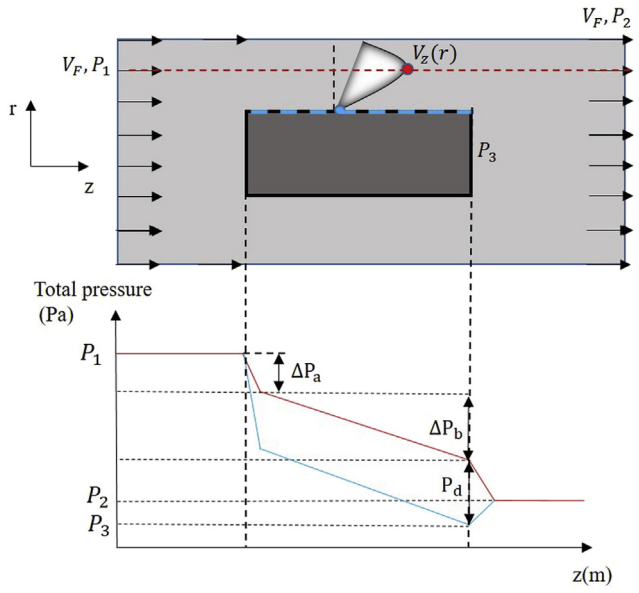

Fig. 3. The total pressure of fluid for the length of the FAST in Lagrangian coordinates.

fluid when the fluid flows to its side area A_s. Fig. 3 shows the Lagrangian coordinates system where the FAST is fixed in the middle of the domain, and the fluid flows near the FAST. Initially, the fluid enters the inlet with a pressure P_1 and a velocity V_F, which is the same condition as the FAST falls with the velocity V_F.

$$\Delta P_a = K_c \rho_c \frac{V_F^2}{2} \tag{8}$$

The pressure drop ΔP_a is caused as the coolant passes the front region of the FAST because of a sudden change in the flow area. K_c in Eq. (8) is a loss coefficient for sudden contraction [13].

$$\Delta P_b = \frac{dP}{dz} L \tag{9}$$

The fluid pressure P_1 acts on the front surface of FAST. After that, the fluid pressure drops due to the friction as the fluid passes near the FAST sides. The value of the pressure gradient is obtained through the pressure gradient technique. The friction between the fluid and the FAST is proportional to the pressure gradient and the length of FAST Eq. 9.

$$P_d = \rho_c \frac{(V_{max} - V_l)^2}{2} \tag{10}$$

where V_{max} is the maximum fluid velocity, and V_l is the fluid velocity at the FAST wall, which is zero in the Lagrangian coordinates system. As shown in Fig. 3, the dynamic pressure is obtained by Eq. (10) because only static pressure acts on the blue line.

$$F_P = (P_1 - P_3) \times A_f \cong (\Delta P_a + \Delta P_b + P_d) \times A_f \tag{11}$$

The fluid at the end wall of FAST forms a vortex when the cross-sectional area becomes large [14]. Additionally, P_3 acts on the back surface of FAST because P_3 does not include the dynamic pressure P_d, as the fluid velocity is zero at the wall. Finally, the fluid has pressure P_2 and velocity V_F at the outlet. The pressure force F_P is proportional to the front area of FAST A_f and the pressure difference between each end surface of FAST. The pressure force acting on the FAST can be approximately calculated by summation of the contraction, the friction pressure drop and the dynamic pressure Eq. 11.

2.3. Heat transfer model

When the temperature of the fuel rod rises from steady-state conditions, the fuel rod transfers heat to the fluid around the FAST, thereby reducing the buoyancy acting on the FAST. The FAST begins to fall into the active core region when the buoyancy applied to the FAST is lower than gravity. In other words, the coolant temperature determines the amount of reactivity inserted by the FAST. Therefore, it is necessary to calculate the temperature distribution in the active core region, considering the process of heat transfer in the region the FAST belongs to. As the coolant temperature at the bottom of the active core region is lower than that at the top region, thermal stratification exists inside the pin. Thus, the fuel, gap, cladding, and stagnant fluid around the FAST transfer heat by conduction, while the coolant in the subchannel conveys heat through convection as it flows. The following heat transfer model determines the transient temperature distribution in the active core region:

$$\rho c_p \frac{\partial T}{\partial t} = \frac{1}{r}\frac{\partial}{\partial r}\left(kr\frac{\partial T}{\partial r}\right) + \frac{\partial}{\partial z}\left(k\frac{\partial T}{\partial z}\right) + h_v \nabla T + q''' \tag{12}$$

where k is the local thermal conductivity of the fuel rod, and h_v is the heat transfer coefficient. The axial and radial temperature distributions in the fuel rod are obtained by Eq. (12) applied to the entire domain in the subchannel. The left-hand side of Eq. (12) contains the energy storage term. The heat conduction, convection, and generation terms are described on the right-hand side. The convection term on the right-hand side is only valid when considering the heat transfer between the cladding and flow channel. Based on the heat transfer model, an implicit scheme is applied to the finite-difference form of Eq. (12) to numerically determine the temperature distribution [15]. Since the actual direction of heat flow is unknown, the heat flow direction is assumed to be such that all the heat flows from neighboring nodes to a central node [16].

As shown in Fig. 4, the entire domain is divided into N nodes in the radial direction and M nodes in the axial direction. The fuel rod, coolant, and FAST pin regions are included in this domain. The implicit scheme is applied to Eq. (12) at node (i, j) in the domain to calculate the temperature distribution. The numerical equations of heat transfer model in each region are as follows:

Fuel, gap, cladding interior:

$$T_{i,j}^n = -\frac{k_{i,j+\frac{1}{2}}^n}{\alpha_{i,j}^n \Delta l^2} T_{i,j+1}^{n+1} - \frac{k_{i+\frac{1}{2},j}^n r_{i+\frac{1}{2}j}}{r_{i,j}\alpha_{i,j}^n \Delta r^2} T_{i+1,j}^{n+1} - \frac{k_{i-\frac{1}{2},j}^n r_{i-\frac{1}{2}j}}{r_{i,j}\alpha_{i,j}^n \Delta r^2} T_{i-1,j}^{n+1} - \frac{k_{i,j-\frac{1}{2}}^n}{\alpha_{i,j}^n \Delta l^2} T_{i,j-1}^{n+1}$$
$$+ \left(\frac{k_{i,j+\frac{1}{2}}^n}{\alpha_{i,j}^n \Delta l^2} + \frac{k_{i+\frac{1}{2},j}^n r_{i+\frac{1}{2}j}}{r_{i,j}\alpha_{i,j}^n \Delta r^2} + \frac{k_{i-\frac{1}{2},j}^n r_{i-\frac{1}{2}j}}{r_{i,j}\alpha_{i,j}^n \Delta r^2} + \frac{k_{i,j-\frac{1}{2}}^n}{\alpha_{i,j}^n \Delta l^2} + 1 \right) T_{i,j}^{n+1} - \frac{q_{i,j}}{\alpha_{i,j}^n} \tag{13}$$

Interface between the cladding wall and the coolant:

$$T_{i,j}^n = -\frac{k_{i,j+\frac{1}{2}}^n}{\alpha_{i,j}^n \Delta l^2} T_{i,j+1}^{n+1} - h_{v_j} \frac{A_{i+\frac{1}{2}j}}{\alpha_{i,j}^n} T_{c,j}^{n+1} - \frac{k_{i-\frac{1}{2},j}^n r_{i-\frac{1}{2}j}}{r_{i,j}\alpha_{i,j}^n \Delta r^2} T_{i-1,j}^{n+1} - \frac{k_{i,j-\frac{1}{2}}^n}{\alpha_{i,j}^n \Delta l^2} T_{i,\frac{j-1}{2}}^{n+1}$$
$$+ \left(\frac{k_{i,j+\frac{1}{2}}^n A_{i,\frac{j+1}{2}}}{\alpha_{i,j}^n \Delta l} + h_{v_j} \frac{A_{i+\frac{1}{2}j}}{\alpha_{i,j}^n} + \frac{k_{i-\frac{1}{2},j}^n A_{i-\frac{1}{2}j}}{\alpha_{i,j}^n \Delta r_i} + \frac{k_{i,j-\frac{1}{2}}^n A_{i,\frac{j-1}{2}}}{\alpha_{i,j}^n \Delta l} + 1 \right) T_{i,j}^{n+1} \tag{14}$$

where.

$T_{i,j}^n$ = *temperature of* (i, j) *node at time step* n

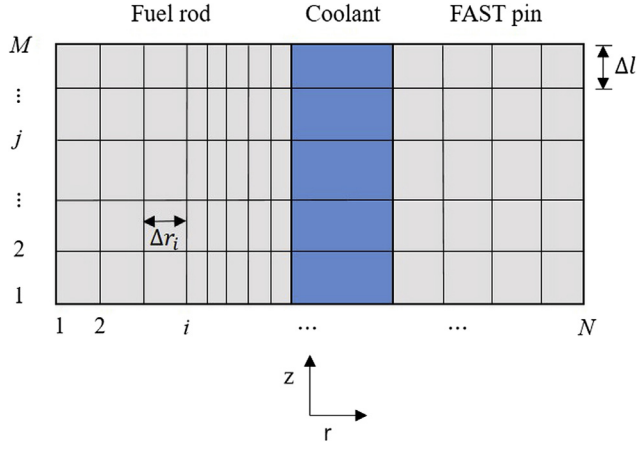

Fig. 4. Nodalization domain of the fuel rod, coolant, and FAST pin.

$T^n_{c,j}$ = coolant temperature at height corresponding to j node
$k^n_{i,j}$ = conductivity (i, j) node at time n
$\alpha^n_{i,j} = \frac{\rho^n_{i,j} c^n_{p_{i,j}} V_{i,j}}{\Delta t}$
$q^n_{i,j}$ = heat generation at (i, j) node at time step n
$A_{i,j}$ = surface area
$\Delta r_{i+\frac{1}{2}}$ = distance between $i+1$ and i node

In Eq. (13), the heat transfer in both radial and axial directions inside the fuel rod is considered. Eq. (14) includes convective heat transfer term, which can be applied to between the coolant and the cladding wall. Insulation is assumed as one of the boundary conditions at $j = M$ and $j = 1$. In the fuel rod centerline, the temperature is calculated by applying the adiabatic condition.

$$h^n_j = h^{n+1}_j + \frac{G\Delta t}{\rho^n_{c,j}\Delta l}\left(h^{n+1}_j - h^{n+1}_{j-1}\right) - \frac{A_H \Delta t}{\rho^n_{c,j} A_F \Delta l} q'' \tag{15}$$

where.

h^n_j = enthalpy of j node at time step n
A_H = heated area
A_F = flow area
q'' = heat flux
G = Mass flux

The energy conservation formula with an implicit scheme is expressed by Eq. (15) in the coolant channel [17]. The mass flow rate along the coolant channel is constant. Therefore, coolant mixing or energy exchange between adjacent channels is not considered. Unlike other regions, the coolant channel has been discretized only in the axial direction. The same procedure is available for the temperature distribution in the pin area containing the FAST.

2.4. Reactor point kinetics model

In this study, the numerical equation of reactor point kinetics is used to calculate the transient behavior of the reactor thermal power by considering one-group point kinetics equations including two differential equations. These equations are derived from the point kinetics equations for six delayed groups [18]. The point kinetics equations are expressed by Eqs. (16) and (17).

$$\frac{dn}{dt} = \frac{\rho(t) - \beta}{\Lambda} n(t) + \lambda C(t) \tag{16}$$

$$\frac{dC}{dt} = \frac{\beta}{\Lambda} n(t) - \lambda C(t) \tag{17}$$

The equations define the reactor thermal power. Under critical conditions, the reactivity is equal to zero. The thermal power is proportional to the neutrons density n generated by a fission process and the decay of the precursor concentration C. The precursors are continuously generated by neutrons, and a decay process reduces the precursors. The specific values for kinetics parameters, such as delayed neutron fraction β and neutron generation time Λ are the same as the values indicated in Hartanto et al. [1].

$$n(0) = n_0 \tag{18}$$

$$C(0) = \frac{\beta}{\lambda \Lambda} n_0 \tag{19}$$

The simulation starts with initial conditions for the neutron density and the precursor concentration as denoted in Eqs. (18) and (19). In this study, the initial conditions are the steady-state conditions just before an accident occurs. With these initial conditions, the numerical solution for Eqs. (16) and (17) can be obtained by applying an implicit time method to the finite differential scheme of the reactor point kinetics equations.

$$n(t+dt) = \frac{n(t) + \lambda \Delta t C(t)}{1 + \frac{\beta - \rho}{\Lambda}\Delta t} \tag{20}$$

$$C(t+dt) = \frac{\frac{\beta \Delta t}{\Lambda} n(t+dt) + C(t)}{1 + \lambda \Delta t} \tag{21}$$

Eqs. (20) and (21) are the implicit numerical equations of reactor point kinetics. The equations are stable as long as the reactivity is negative. The time step used in this study is small enough to maintain the accurate simulation results without instability even if the reactivity in the reactor system is positive.

$$\rho_t(t) = \rho_{ab}(t) + \alpha_{Doppler}\left(\overline{T_f}(t) - \overline{T_f}(0)\right) + (\alpha_{Na} + \alpha_{Axial} + \alpha_{CEDL} + \alpha_{Radial})(\overline{T_c}(t) - \overline{T_c}(0)) \tag{22}$$

The total reactivity ρ_t consists of the reactivity introduced by the FAST ρ_{ab} and various reactivity feedback due to the variation of the average fuel temperature $\overline{T_f}$ and average coolant temperature $\overline{T_c}$ [19]. Eq. (22) considers the reactivity feedback terms including the coefficient of fuel temperature reactivity feedback $\alpha_{Doppler}$, sodium temperature reactivity feedback α_{Na}, axial expansion reactivity feedback α_{Axial}, control assembly driveline expansion reactivity feedback α_{CEDL} and radial expansion reactivity feedback α_{Radial}.

3. Simulation conditions to evaluate the performance of FAST

The two central objectives of the FAST system is to reduce the value of CVR in LOCA condition and to insert negative reactivity under transient conditions. Hartanto et al. [1] mainly focused on evaluating the contribution of the FAST system to lowering the CVR effect when the coolant forms void. According to the authors, the FAST system could reduce approximately 2.5 $ of CVR under LOCA conditions. However, there is still a need to evaluate the FAST system under transient conditions that are completely different from the LOCA conditions. When the FAST is applied to iSFR, the FAST adjusts the total reactivity and thermal power depending on its position. Therefore, the FAST with the current design should be simulated under transient conditions. The fuel shape was a cylinder with a radius of 0.4298 cm as the annular fuel becomes the cylindrical fuel with the fuel burnup and thermal expansion. The reactor core includes a 100 cm LEU driver region and a 30 cm axial blanket located in each end side. In addition, the heat generation in the fuel rod was defined with a cosine axial power shape. The number of nuclear fuel rods in each assembly was 214, where 3 of 217 fuel rods are replaced with the FASTs in only inner fuel assemblies. The mass flux was 2105 kg/m^2s to make the average core outlet temperature 663 K under the conditions listed in Table 1.

Among the total assemblies including inner and outer fuel assemblies, the FAST modules are equipped in each inner fuel assembly where the normalized radial power distribution varies from 0.866 to 1.069 at BOL [1]. The EOL condition makes a large difference in normalized radial power varying from 0.889 to 1.282 in the inner fuel assemblies. The normalized radial power of the iSFR core in only inner fuel assemblies was aligned to the descending order in Fig. 5.

The kinetics parameters and reactivity feedback coefficients at BOL and EOL are listed in Table 2. The parameters change slightly as the initial fuel with U-235 turns into transuranic elements with fuel

Table 1
Main design parameter of the iSFR.

Design parameter	Value
Core power, MWth	392.6
Active core length, cm	100
Coolant inlet temperature, K	663
Coolant outlet temperature, K	818
Number of fuel assemblies	144
Number of fuel rods in each assembly	214
Fuel pin diameter, cm	0.9675
Fuel radius, cm	0.4298
Gap thickness, cm	0.004
Cladding thickness in the fuel rod, cm	0.05
P/D ratio	1.14
Mass flux, kg/m^2s	2105
FAST diameter, cm	0.62
FAST height, cm	170.04
Absorber height, cm	100
Void height, cm	70
Cladding thickness in the FAST, cm	0.01
Number of inner fuel assembly	84
Number of outer fuel assembly	60
Number of primary control assembly	4
Number of secondary control assembly	3

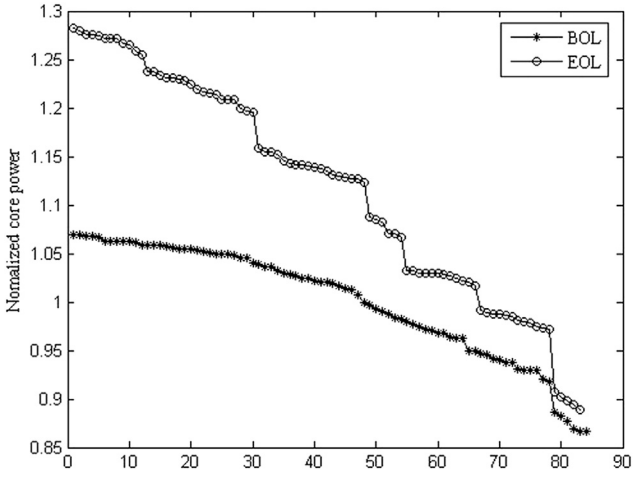

Fig. 5. The normalized radial power distribution in inner fuel assemblies at BOL and EOL.

Table 2
Reactivity feedback coefficients and kinetics parameters at BOL and BOL [1].

Design parameter	Value at BOL	Value at EOL
$\alpha_{Doppler}$, ¢/K	−0.056	−0.072
α_{Na}, ¢/K	−0.011	0.201
α_{Axial}, ¢/K	−0.029	−0.060
α_{CEDL}, ¢/K	−0.015	−0.063
α_{Radial}, ¢/K	−0.116	−0.153
β, ¢	0.0071	0.0044
λ, sec^{-1}	0.077	0.077
Λ, μsec	1.025	0.768
Total worth of the FAST system, ¢	−234.5	−312.4[a]

[a] 20% B-10 depleted.

burnup. The thermal conductivity, density and heat capacity for U–7Zr metallic fuel and HT-9 cladding were interpolated, and the thermal properties of the sodium coolant were used in response to the temperature [3,20,21].

Among the design basis accidents (DBAs), a single control rod withdrawal accident, which is a bounding event of DBA Class 2 in the PGSFR, was adopted to give transient overpower conditions

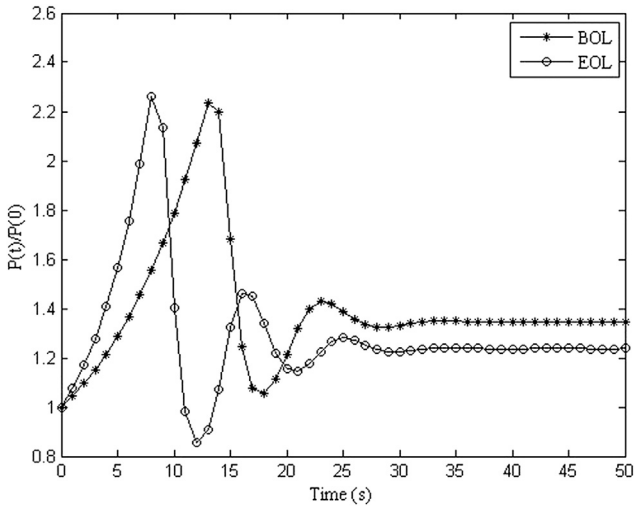

Fig. 6. The reactor thermal power ratio for 50 s immediately after the accident.

[22]. The event was defined to linearly insert a positive reactivity of 68.7¢ for 15 s. This event describes transition conditions that increase the reactor thermal power and overall system temperature. Among accidents that happen in PGSFR, the acceptance criteria for DBA Class 2 are based on the fuel, cladding and coolant temperature. Accordingly, the assumed event makes it possible to evaluate the performance of the FAST on the temperature and thermal power under both BOL and EOL conditions. Basically, the reactor was supposed to trip at 2.22 s when a high-power-to-flow rate ratio is detected. However, the reactor trip conditions were not used to evaluate the performance of FAST alone.

Since the simulations for the current FAST design have not yet been conducted, it is necessary to investigate how the FAST behaves with the given conditions increasing the coolant temperature. In this study, simulations were performed to take into account the temperature distribution over the entire fuel assembly, causing FAST to insert negative reactivity at different moments. The FAST in the hottest fuel assembly is expected to fall faster than the FAST in the coldest fuel assembly. This difference in insertion time may lead to gradual reactivity insertion in the active core region. Based on these considerations, the FAST position, power ratio, reactivity, maximum subchannel temperature and applicability of FAST to iSFR are discussed.

4. Results and discussion

The simulation starts from the steady-state conditions and continues for 50 s. When the reactor is in the steady-state conditions, the coolant outlet temperature in inner fuel assemblies is distributed 797–832 K at BOL and 801–861 K at EOL.

Fig. 6 indicates the reactor thermal power ratio where $P(0)$ is the initial reactor thermal power in the steady-state condition. Fig. 7 exhibits the total reactivity controlled by the reactivity feedback and the FAST system. Immediately after the accident has occurred, the thermal power starts to rise steeply as the accident introduces the positive reactivity. When the reactor power is almost 2.25 times the initial power $P(0)$, the power decreases rapidly due to the negative reactivity inserted by the FASTs. Specifically, the reactor core begins to be affected by the FAST when it arrives at 1.7 m height. Since the FASTs insert a large amount of negative reactivity in the reactor core, the coolant temperature drops suddenly and the buoyancy acting on the FAST increases. The FAST sinks more to where the buoyancy is greater than gravity because of the inertia

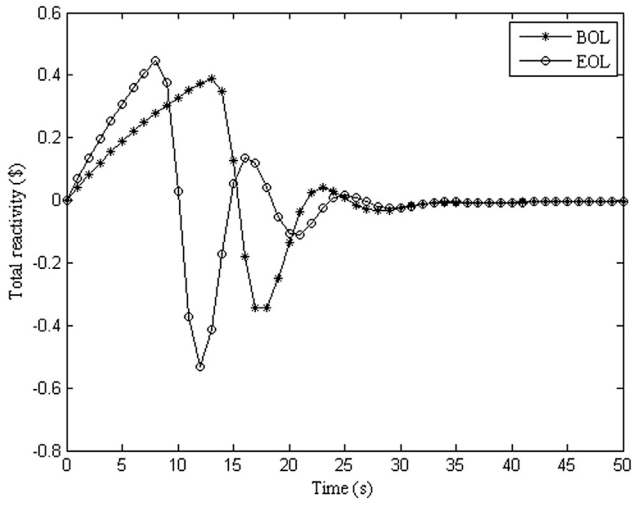

Fig. 7. Total reactivity for 50 s immediately after the accident.

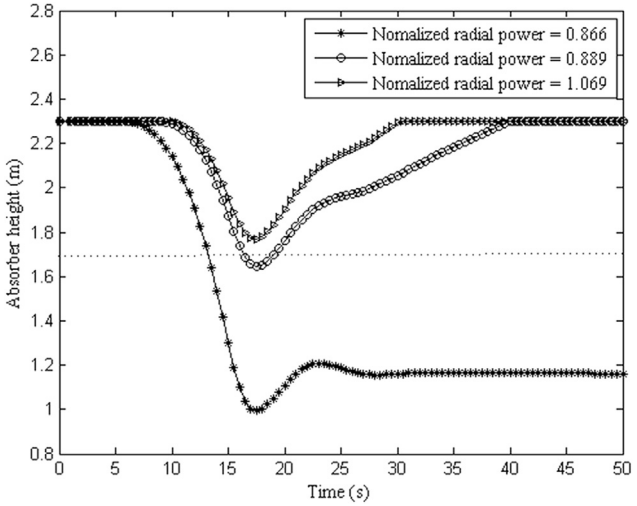

Fig. 8. Absorber height for 50 s after the accident at BOL.

although buoyancy is greater than gravity. Therefore, the FAST rises again and inserts the positive reactivity, leaving the active core region. This FAST movement repeatedly increases and decreases the reactor power.

During the entire simulation, the reactivity feedback not only prevents a rapid increase in thermal power at the beginning of the accident, but also it reduces the amplitude of the thermal power. The thermal power at EOL rises more steeply because the sum of reactivity coefficients for EOL is greater than that for BOL. For example, CTC, which had a negative value in BOL, has a positive value at EOL. Interestingly, it was observed that the reactor power does not return to its initial value for 50 s despite the FAST insertion. It means that even if the FAST inserts negative reactivity, the reactor power is not the same as before. Specifically, Eqs. (16) and (17) prove that the initial power P(0) cannot be obtained when the same amount of negative reactivity is added after the positive reactivity has been inserted. This behavior significantly contrasts when the reactor core is shut down by the control rod system. Unlike the control rod system, the FAST could not reduce the reactor thermal power to its initial state because it precisely inserts negative reactivity as much as the positive reactivity inserted by accident. To lower the reactor power below the initial power, the FAST should cooperate with other safety systems such as the control rod system.

The behavior of FAST considerably affects the reactor core power. Thus, the absorber height was tracked for 50 s because the absorber height, rather than the FAST height, determines the reactivity inserted by the FAST. Fig. 8 shows the temporal evolution of the absorber height for various normalized radial power distributions. As the FASTs are supposedly designed, all FASTs are located outside the active core region under the steady-state conditions. The FAST is designed to fall when the coolant outlet temperature reaches 870 K. Under the given accident conditions at BOL, it takes approximately 7 s for the coolant outlet temperature to exceeds 870 K in the hottest fuel assembly, where the normalized radial power is 1.069. After the FAST reaches 1.7 m of the active core region, a large amount of negative reactivity is inserted. Interestingly, the FASTs, located where the normalized radial power is less than 0.889, are still above the active core region and cannot contribute to controlling the reactor thermal power because the coolant temperature is relatively low in normal operation. Secondly, the FASTs in the hot fuel assemblies cool down the coolant before the other FASTs in the cold fuel assemblies arrive at the active core region. The EOL conditions show slightly different FAST behaviors (Fig. 9). The FAST in the hottest fuel assembly begins to fall about 3 s following the accident because the coolant outlet temperature is already 861 K under steady-state conditions. Therefore, if the coolant rises only 9 K under the steady-state conditions, then FAST starts to fall. This small temperature margin may allow the FAST to insert the negative reactivity before the accident occurs. Therefore, the current FAST density should be reduced to avoid inserting unnecessary reactivity. On the other hand, the FASTs are still above 1.7 m height, where the normalized radial power is less than 0.972. In this range, the FAST density should increase to insert negative reactivity. This result indicates that the current FAST performances can be improved by adjusting the FAST density depending on its installed location. Therefore, further study with more focus on design optimization for the FAST system should be undertaken.

The fuel, cladding and coolant temperature are important factors as they are the safety criteria of the DBA Class 2 event. Fig. 6 shows that the thermal power is higher than the initial thermal power even after the thermal power has been stabilized. The maximum fuel and cladding temperatures show a similar trend with the reactor thermal power (Figs. 10 and 11). According to the

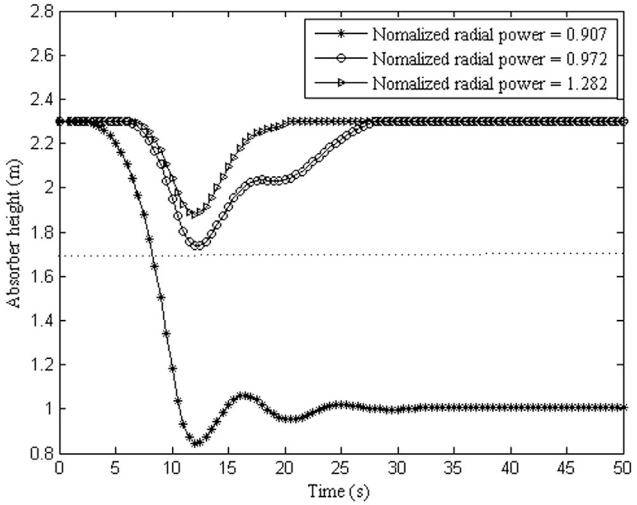

Fig. 9. Absorber height for 50 s after the accident at EOL.

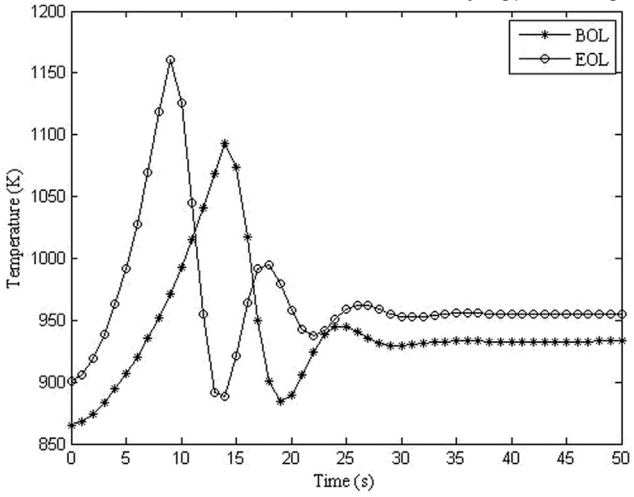

Fig. 10. Maximum fuel rod temperature in the entire fuel assembly including inner and outer fuel assemblies.

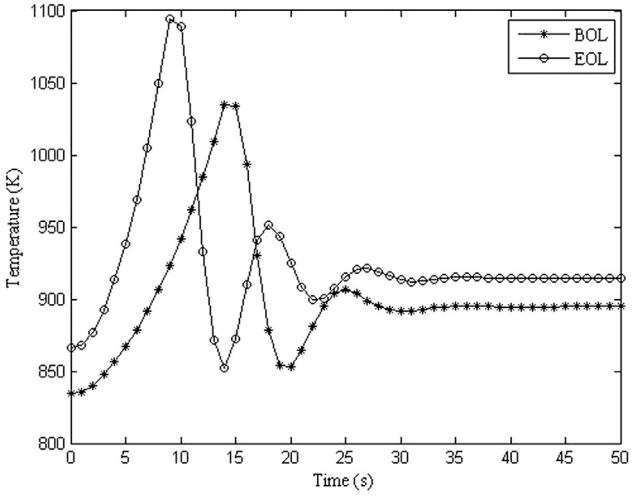

Fig. 11. Maximum cladding temperature in the entire fuel assembly including inner and outer fuel assemblies.

safety acceptance criteria for DBA Class 2 event, the fuel rod temperature should be kept below its melting temperature, and the coolant temperature should be lower than its boiling temperature [22]. From the data in Fig. 10, the maximum fuel temperature for U–7Zr is below its solidus temperature of 1420 K [23]. There is no significant difference between the fuel and cladding temperatures owing to the high thermal conductivity of the metallic fuel. The maximum temperature difference between the fuel and cladding is only approximately 60 K at BOL and 72 K at EOL. The HT-9 cladding has excellent resistance to swelling and creep up to 923 K. Meanwhile, the neutron irradiation makes the ductile-brittle transition temperature increase quickly below 673 K [24]. It means that the cladding temperature should be between 673 K and 923 K to avoid the low-temperature irradiation embrittlement and to achieve a satisfactory creep performance. Even though the peak cladding temperature exceeds 923 K for 10 s, this exposure time is too short to develop complete secondary phases in HT-9 cladding [25]. When it comes to changing the temperature, quickly stabilizing the reactor power is important because the cyclical thermal loading coupled with the mechanical loading, such as the turbulent flow of the coolant and fission products inside the fuel rods, may accelerate the failure progress. The FAST keeps the reactor stable within 35 s,

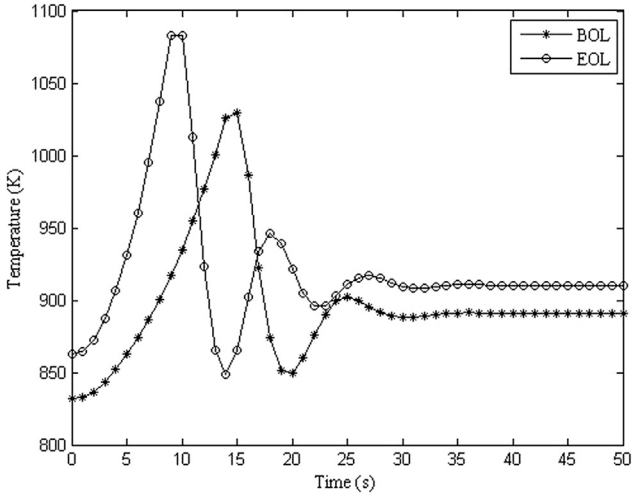

Fig. 12. Maximum coolant temperature in the entire fuel assemblies including inner and outer fuel assemblies.

giving a low periodic thermal load to the fuel rod.

The results, as shown in Fig. 12, indicate that the FAST alone is enough to meet the safety acceptance criteria in terms of the coolant boiling limit temperature of 1156 K at EOL, without any help of other safety systems. However, once the voids are formed, the reactor thermal power rises due to positive reactivity insertion at EOL. The maximum coolant temperature is 1033 K at BOL and 1091 K at EOL respectively. In order to lower the maximum coolant temperature in an accident, the FAST should reach the active core region more quickly during an accident. To this end, reducing the distance of 0.6 m between the absorber and the active core region can be one of the alternatives to respond quickly to changes in the reactor thermal power although the boron carbide is more depleted by neutron absorption.

5. Conclusion

The FAST is a passive safety device used to reduce CVR without changing the reactor core geometry and to insert negative reactivity under transient conditions. There are a total of 252 FASTs only in the inner fuel assemblies. Each FAST is located outside the active core region to reduce neutron leakage under the steady-state conditions. Moreover, the FAST can insert negative reactivity into the reactor by gravity in case of LOCA. However, the FAST system has not been evaluated under transient conditions so that it can be applied to an actual system. Especially, the actual behavior of the FAST is unclear under transient conditions increasing the reactor core power or coolant temperature. Therefore, the previous FASTAC has been improved to simulate the behavior of the FAST by considering models for the temperature distribution and reactivity insertion in the reactor core under the single control rod withdrawal accident. The implemented models in FASTAC described the forces acting on the FAST, reactor point kinetics and temperature distribution in the fuel assemblies with different radial core powers.

With the previously mentioned analysis models, the current FAST system was simulated at BOL and EOL during an accident. This study focused on the FAST movement when the coolant temperature increases, simulating transient conditions in the reactor core. The accident was assumed to linearly insert a positive reactivity of 68.7¢ for 15 s. Other safety devices or systems were not considered to assess the performance of the FAST system alone. The increase in

initial reactor thermal power was restrained by negative reactivity feedback. Once the FAST reached the active core region, the reactor thermal power was abruptly reduced by the insertion of negative reactivity. After the FAST fell, the FAST began to oscillate due to sudden changes in the buoyancy acting on the FAST. Unlike the control rod systems, the reactor thermal power could not return to its initial state because the FAST precisely inserts negative reactivity as much as the positive reactivity caused by the accident. These results imply that the FAST system cannot independently shut down the reactor core. Therefore, it is necessary to use additional safety devices, such as a control rod system, to reduce the reactor thermal power below the initial state when the positive reactivity is inserted.

The location of all FAST installed in the inner fuel assemblies was analyzed for 50 s after the accident. Under EOL conditions, the FAST in the hottest fuel assembly began to fall quickly in 3 s after the accident. These results suggested the possibility of unnecessary insertion of the negative reactivity in normal operation since only a 9 K of temperature margin remains until the FAST begins to move. On the other hand, FASTs installed at relatively low powers were not useful while the thermal power increased about 2.25 times initial power. It is necessary to adjust the FAST density depending on its installed location to avoid inserting unnecessary negative reactivity and to make the FAST more useful. To this end, further study on optimization for the FAST system should be needed under various accident conditions.

Regarding the safety criteria, the FAST met the safety acceptance criteria for DBA Class 2 accident mainly based on the pin melting temperature and coolant boiling temperature. The FAST system maintained satisfactory temperatures for both the fuel rod and the coolant. The maximum fuel temperature was 1093 K at BOL and 1161 K at EOL. The cladding temperature reached peak temperature with the thermal power. Although cladding temperature exceeded its limit temperature for approximately 10 s at BOL and EOL, it was not a concerning issue as long as the cladding temperature was maintained within a satisfactory temperature within a few seconds. Moreover, the FAST system alone was sufficient to cool the coolant to temperatures below the boiling temperature of sodium. Based on the simulation results, the current FAST system showed outstanding performance in terms of quickly stabilizing the reactor core under the given transient conditions, without any help of other safety systems. Besides, the FAST is expected to similarly operate under other accidents that increase the overall system temperature. It appears feasible to use the FAST system in iSFR to satisfy the safety criteria with given accident conditions.

Declaration of competing interest

No conflicts of interest.

Acknowledgements

This work was supported by the National Research Foundation of Korea (NRF) grant funded by the Korean government (Ministry of Science and ICT) (No. NRF-2017M2B2B1071971).

Nomenclature and units

A_F	coolant flow area (m^2)
A_f	FAST front area (m^2)
A_H	coolant heated area (m^2)
A_s	FAST side area (m^2)
C	precursors concentration
c_p	heat capacity (J/kg·K)
F_B	buoyancy (Pa/m^2)
F_D	drag (Pa/m^2)
F_G	gravity (Pa/m^2)
F_P	pressure force (Pa/m^2)
G	mass flux (m^2/s)
g	gravitational acceleration (m/s^2)
h	enthalpy (J/kg)
h_v	heat transfer coefficient ($W/m^2 \cdot K$)
K_c	loss coefficient for sudden contraction
k	thermal conductivity (W/m·K)
L	FAST length (m)
Δl	height difference (m)
n	neutrons density
P	pressure (Pa)
P_1	fluid pressure at inlet (Pa)
P_2	fluid pressure at outlet (Pa)
P_3	fluid pressure at back surface of FAST (Pa)
ΔP_a	pressure drop by sudden contraction (Pa)
ΔP_b	pressure drop by friction (Pa)
P_d	fluid dynamic pressure (Pa)
Q	coolant volumetric flow (m^3/s)
Q_e	estimated coolant volumetric flow (m^3/s)
q''	heat flux (W/m^2)
q'''	volumetric heat generation (W/m^3)
r	radius (m)
r_F	FAST radius (m)
r_p	pin radius (m)
T	temperature (K)
$\overline{T_c}$	average coolant temperature (K)
$\overline{T_f}$	average fuel temperature (K)
t	time (s)
Δt	time step (s)
V	FAST volume (m^3)
V_F	FAST velocity (m/s)
V_l	fluid velocity at the FAST wall for the Lagrangian coordinates system (m/s)
V_{max}	fluid maximum velocity (m/s)
V_z	(r) velocity function (m/s)

Greek symbols

Λ	neutron generation time (s)
α_{Axial}	axial expansion reactivity coefficient
α_{CEDL}	control assembly driveline expansion reactivity coefficient
$\alpha_{Doppler}$	Doppler reactivity coefficient
α_{Na}	sodium temperature reactivity coefficient
α_{Radial}	radial expansion reactivity coefficient
β	delayed neutron fraction
Λ	prompt neutron generation time (s)
μ	coolant viscosity (Pa·s)
ρ	density (kg/m^3), reactivity
ρ_{ab}	reactivity inserted by the FAST
ρ_c	coolant density (kg/m^3)
ρ_F	FAST density (kg/m^3)
ρ_t	total reactivity
ρ_F	FAST density (kg/m^3)

Subscripts

0	initial or steady state
1	inlet
2	outlet
3	back surface of the FAST
c	coolant
e	estimated
F	FAST

f	fuel, front
i, j	nodal point in some domain
l	Lagrangian coordinates system
n	time step
p	pin
r	radius
s	side
t	total

References

[1] D. Hartanto, I. Kim, C. Kim, Y. Kim, An LEU-loaded long-life innovative sodium-cooled fast reactor (iSFR) with novel and passive safety devices, Ann. Nucl. Energy 95 (2016) 86–101, https://doi.org/10.1016/j.anucene.2016.04.051.

[2] W.S. Yang, Fast reactor physics and computational methods, Nucl. Eng. Technol. 44 (2012) 177–198, https://doi.org/10.5516/NET.01.2012.504.

[3] D.G. Cacuci, Handbook of Nuclear Engineering, Springer Science & Business Media, New York, 2010.

[4] B. Merk, Fine distributed moderating material with improved thermal stability applied to enhance the feedback effects in SFR cores, Sci. Technol. Nucl. Install. 2013 (2013) 1–11, https://doi.org/10.1155/2013/217548.

[5] S.J. Kim, N.Z. Cho, Y.J. Kim, A pan-shape transuranic burner core with a low sodium void worth, Ann. Nucl. Energy 27 (2000) 435–448, https://doi.org/10.1016/S0306-4549(99)00101-2.

[6] C. Sciora, P., D. Blanchet, L. Buiron, B. Fontaine, M. Vanier, F. Varaine, Venard, Low void effect core design applied on 2400 MWth SFR reactor, in: International Congress on Advanced Nuclear Power Plants, Nice, France, 2011. May 2–5.

[7] M.F. Khalil, S.Z. Kassab, I.G. Adam, M. Samaha, Laminar flow in concentric annulus with a moving core, in: International Water Technology Conference, 2008. Alexandria, Egypt, March 27-30.

[8] I. Kim, T.F. Irvine, N.A. Park, Experimental study of the velocity field around a falling needle viscometer, Rev. Sci. Instrum. 65 (1994) 224–228, https://doi.org/10.1063/1.1144789.

[9] E.G. Wehbeh, T.J. Ui, R.G. Hussey, End effects for the falling cylinder viscometer, Phys. Fluids A Fluid Dyn. 5 (2002) 25–33, https://doi.org/10.1063/1.858781.

[10] M.C.S. Chen, J.A. Lescarboura, G.W. Swift, The effect of eccentricity on the terminal velocity of the cylinder in a falling cylinder viscometer, AIChE J. 14 (1968) 123–127, https://doi.org/10.1002/aic.690140122.

[11] S. Lee, Y.H. Jeong, Floating absorber for safety at transient analysis code (FASTAC): verification and validation study, in: International Topical Meeting on Nuclear Reactor Thermal-Hydraulics, Opereration and Safety, 2018. Qingdao, China, October 14-18.

[12] S.V. Patankar, Numerical Heat Transfer and Fluid Flow, first ed., CRC Press, Boca Raton, 1980.

[13] F.M. White, Fluid Mechanics, seventh ed., McGraw-Hill, New York, 2011.

[14] G. Biswas, M. Breuer, F. Durst, Backward-facing step flows for various expansion ratios at low and moderate Reynolds numbers, J. Fluids Eng. 126 (2004) 362–374, https://doi.org/10.1115/1.1760532.

[15] R.H. Anderson, D. Tannehill, J.C. Pletcher, Computational Fluid Mechanics and Heat Transfer, third ed., CRC Press, Boca Raton, 2016 https://doi.org/10.1201/b12884.

[16] A.S. Incropera, F.P., D.P. DeWitt, T.L. Bergman, Lavine, Foundations of Heat Transfer : International Student Version, sixth ed., John Wiley & Sons Ltd, 2012.

[17] H. Kazeminejad, Thermal–hydraulic modeling of reactivity insertion in a research reactor, Ann. Nucl. Energy 45 (2012) 59–67, https://doi.org/10.1016/j.anucene.2012.02.017.

[18] J.R. Lamarsh, A.J. Baratta, Introduction to Nuclear Engineering, third ed., Prentice hall, Upper Saddle River, New Jersey, 2001.

[19] C. Housiadas, Lumped parameters analysis of coupled kinetics and thermal-hydraulics for small reactors, Ann. Nucl. Energy 29 (2002) 1315–1325, https://doi.org/10.1016/S0306-4549(01)00107-4.

[20] L. Leibowitz, R.A. Blomquist, Thermal conductivity and thermal expansion of stainless steels D9 and HT9, Int. J. Thermophys. 9 (1988) 873–883, https://doi.org/10.1007/BF00503252.

[21] Y.S. Touloukian, R.W. Powell, C.Y. Ho, P.G. Klemens, Thermophysical Properties of Matter - the TPRC Data Series. Volume 1. Thermal Conductivity - Metallic Elements and Alloys, Plenum Press, New York, 1970.

[22] K.L. Lee, K.S. Ha, J.H. Jeong, C.W. Choi, T. Jeong, S.J. Ahn, S.W. Lee, W.P. Chang, S.H. Kang, J. Yoo, A preliminary safety analysis for the prototype gen IV sodium-cooled fast reactor, Nucl. Eng. Technol. 48 (2016) 1071–1082, https://doi.org/10.1016/j.net.2016.08.002.

[23] M.S. Dias, J.R.L.D, Mattos, Uranium-zirconium based alloys part I: reference points for thermophysical properties, in: International Nuclear Atlantic Conference, (São)

[24] Y. Chen, Irradiation effects of HT-9 martensitic steel, Nucl. Eng. Technol. 45 (2013) 311–322, https://doi.org/10.5516/NET.07.2013.706.

[25] R. Klueh, D. Harries, High-Chromium Ferritic and Martensitic Steels for Nuclear Applications, ASTM International, West Conshohocken, 2011.